
Graph Learning with Distributional Edge Layouts

Xinjian Zhao¹ Chaolong Ying¹ Tianshu Yu¹

Abstract

Graph Neural Networks (GNNs) learn from graph-structured data by passing local messages between neighboring nodes along edges on certain topological layouts. Typically, these topological layouts in modern GNNs are deterministically computed (e.g., attention-based GNNs) or locally sampled (e.g., GraphSage) under heuristic assumptions. In this paper, we for the first time pose that these layouts can be globally sampled via Langevin dynamics following Boltzmann distribution equipped with explicit physical energy, leading to higher feasibility in the physical world. We argue that such a collection of sampled/optimized layouts can capture the wide energy distribution and bring extra expressivity on top of WL-test, therefore easing downstream tasks. As such, we propose Distributional Edge Layouts (DELs) to serve as a complement to a variety of GNNs. DEL is a pre-processing strategy independent of subsequent GNN variants, thus being highly flexible. Experimental results demonstrate that DELs consistently and substantially improve a series of GNN baselines, achieving state-of-the-art performance on multiple datasets.

1. Introduction

Graph neural networks (GNNs), which learn informative knowledge from graph-structured data, have witnessed remarkable success in a large variety of applications, such as molecular generation (Jin et al., 2018), link prediction (Zhang & Chen, 2018), to name a few. A standard learning paradigm in GNNs is the message-passing mechanism, which takes node/edge features as inputs and propagates messages through neighboring nodes defined on some topological layouts (Wu et al., 2020). Given a graph $\mathcal{G} = (\mathbf{H}^{(0)}, \mathbf{A})$ where $\mathbf{H}^{(0)}$ and \mathbf{A} are respectively initial features and connectivity, GNNs seek to learn meaningful

representations by stacking multiple unit layers. Concretely, for almost all variants of GNNs, an update layer can be generalized as (Balcilar et al., 2021a):

$$\mathbf{H}^{(l+1)} = \sigma \left(\sum_s \mathbf{C}^{(s)} \mathbf{H}^{(l)} \mathbf{W}^{(l,s)} \right) \quad (1)$$

where $\mathbf{H}^{(l)} \in \mathbb{R}^{n \times f_l}$ refers to the feature at l -th layer. $\mathbf{C}^{(s)} \in \mathbb{R}^{n \times n}$ is the s -th topological layout on which messages are propagated between neighboring nodes, and $\mathbf{W}^{(l,s)} \in \mathbb{R}^{f_l \times f_{l+1}}$ is the learnable parameter at the l -th layer and s -th layout. $\sigma(\cdot)$ is a non-linear activation function. It is argued in Bouritsas et al. (2022) that GNNs generally differ from each other by the choice of layouts $\mathbf{C}^{(s)}$.

Early GNNs utilize a direct mapping of original input connectivity \mathbf{A} as the topological layout (Kipf & Welling, 2016; Yu et al., 2019), which may result in sub-optimal performance. Stronger GNNs in general focus on designing a more sophisticated layout set $\mathbf{C}^{(s)}$ to decouple the computational layout from the raw graph, bringing about benefits for downstream tasks accordingly. Several aspects have been considered in this line of methods, such as spectral information (Huang et al., 2022), expressivity (Xu et al., 2019b), and attention mechanism (Veličković et al., 2018; Wu et al., 2021; Rampášek et al., 2022). Among these branches, attention-based GNNs may be the most successful, delivering state-of-the-art performance on a range of public datasets (Rampášek et al., 2022; Zhang et al., 2022). Subgraph sampling, in parallel, is also employed to produce topological layouts, by incorporating locality-based randomness, such as random walk (Hamilton et al., 2017) and edge rewiring/dropping (Rong et al., 2020).

We note that existing GNNs obtain topological supports either through deterministic mappings or by injecting randomness locally. In the real world, however, layouts associated with a given graph may span over a wide potential distribution under some global criteria. For example, 3D conformations given a molecule atom-bond graph tend to exist in the physical world following Boltzmann distribution with a global free energy (Xu et al., 2021). Thus, deriving a single conformation is insufficient to holistically capture the potential energy surface, bringing about difficulty for subsequent tasks. Motivated by this, in this paper, we propose to cope with layouts by introducing an associated distribution

*Equal contribution ¹School of Data Science, The Chinese University of Hong Kong, Shenzhen. Correspondence to: Tianshu Yu <yutianshu@cuhk.edu.cn>.

over \mathbf{C} :

$$\mathbf{H}^{(l+1)} = \sigma \left(\int \mathbf{C} \mathbf{H}^{(l)} \mathbf{W}^{(l)} d\mathbb{P}(\mathbf{C}) \right) \quad (2)$$

where $\mathbb{P}(\mathbf{C})$ is the probability density of occurrence of \mathbf{C} and is related to some global energy function $E(\mathbf{C})$. Now two problems remain: 1) what energy and distribution to use; and 2) how to integrate derived layouts into GNNs.

To this end, we draw inspiration from energy-based layout computation in graph visualization (Fruchterman & Reingold, 1991; Kamada et al., 1989; Gansner et al., 2005; Wang et al., 2017). In a nutshell, layouts in graph visualization are diverse and viable configurations in low-dimensional space, explicitly optimized over physics-driven energy functions. A nice property is that it only depends on pure topology/connectivity without requiring node features, which can be flexibly coupled with multiple GNNs. Further motivated by statistical mechanics, we employ Boltzmann distribution defined on such energy to characterize the distribution of layouts \mathbf{C} . To sample from Boltzmann distribution, one can employ Langevin Dynamics to inject proper noise along the optimization trajectory. Empirically, we argue that DELs can produce stable layouts for isomorphic graphs and remarkably distinguishable layouts for non-isomorphic ones, in a sense that extra expressivity beyond WL-test can be obtained from physics. Furthermore, such a collection of layouts can be pre-calculated before fed into standard GNNs. In summary, we propose Distributional Edge Layouts (DELs), which sample layouts from the designated distribution, and flexibly inject this information into a series of GNNs as supplements. Experimentally, we observe that DEL can improve the learning performance of selected GNNs by a large margin on a wide range of datasets, demonstrating strong applicability and flexibility. In conclusion, our contributions are:

- We propose a generic GNN format by sampling topological layouts from Boltzmann distribution with explicit energy surface, which can capture a wide spectrum of global graph information.
- Calculation of DELs is independent of GNNs, leading to high flexibility and applicability.
- As a plug-in component, DELs substantially improve selected GNNs, achieving state-of-the-art performance on a variety of datasets.

2. Related Work

Graph Neural Networks with topological layout. It has been argued by Bouritsas et al. (2022); Balcilar et al. (2021b) that the topological layout, represented as \mathbf{C} , determines the specific way of message passing between nodes. By default,

connectivity \mathbf{A} itself defines a layout, while a naive layout yields unsatisfactory performance. A series of GNNs then seek to directly transform \mathbf{A} , from either spatial or spectral perspectives (Kipf & Welling, 2016; Xu et al., 2019a; Defferrard et al., 2016; Dwivedi & Bresson, 2021; Kreuzer et al., 2021). Sampling/rewiring-based GNNs, in parallel, are further proposed by advocating local randomness on \mathbf{C} , bringing about higher robustness (Alon & Yahav, 2020; Topping et al., 2022; Rong et al., 2020). Many other GNNs also consider deriving \mathbf{C} from an “edge feature” aspect, as \mathbf{C} inherently aligns with some edge layout. For instance, EGNN (Gong & Cheng, 2019) tackles this challenge by constructing edge features based on the direction of directed edges in citation networks. Similarly, Sun et al. (2022) proposes leveraging chemical properties like bond types and bond directions to create edge features for molecular graphs. Circuit-GNN, introduced by Zhang et al. (2019), is tailored for distributed circuit design. In Circuit-GNN, nodes represent resonators, and edges denote electromagnetic couplings between pairs of resonators. These edge features are derived from physical circuit characteristics, including gap, shift, and relative position between square resonators, among other factors, which contribute to the refinement of topological layouts. Although some general edge feature construction schemes exist, such as MPNN (Gilmer et al., 2017), Point-GNN (Shi & Rajkumar, 2020), and CIE (Yu et al., 2019), they generate edge features through node features in a heuristic fashion without physical implication.

Graph layout algorithm. Graph layout algorithms arrange nodes and edges in low-dimensional space to depict viable graph topology. It is widely applicable in domains like social network analysis (Henry et al., 2007; Wang et al., 2020) and bioinformatics (Sych et al., 2019). Our primary focus is on energy-based layout algorithms (Fruchterman & Reingold, 1991; Kamada et al., 1989; Gansner et al., 2005; Wang et al., 2017), which adapt well to different topologies by simulating the physical interactions between nodes to determine their positions. These methods, rooted in principles of physics, offer a range of configurations in lower-dimensional spaces. Classic energy-based graph layout algorithms typically utilize either a spring model (Kamada et al., 1989; Gansner et al., 2005) or a spring-electrical model (Fruchterman & Reingold, 1991; Jacomy et al., 2014). In the spring model, edges are conceptualized as springs, and relationships between nodes are simulated by the tension in the springs. The spring-electrical model combines the spring model with Coulomb’s law to introduce repulsive forces between nodes, treating nodes as charged particles. These models optimize graph layouts in an iterative manner. More discussion can be found in Appendix B.

3. Preliminary

3.1. Boltzmann Distribution

The Boltzmann distribution (Boltzmann, 1868) plays a crucial role as a probability distribution function in the field of statistical mechanics. Its primary purpose is to quantify the probability of particles residing at specific energy levels. This distribution is commonly employed to describe how particles, such as molecules or atoms, are distributed among different states or energy levels in a system at thermal equilibrium. The mathematical representation of the Boltzmann distribution is as follows:

$$\mathbb{P}(E) = \frac{1}{Z} e^{-\frac{E}{kT}} \quad (3)$$

where $\mathbb{P}(E)$ is the probability of particles being in the energy level E , Z is the normalization constant, known as the partition function, which ensures that the probability distribution sums to 1. T is the temperature of the system in Kelvin, and k is the Boltzmann constant, which used to convert temperature T from Kelvin to energy units.

3.2. Edge-aware GNNs

Most current GNNs primarily emphasize message passing among node features. However, incorporating edge features into GNNs can enhance the topological layout of graphs to better suit downstream tasks. By modifying the element $\mathbf{C}_{v,u}^l$ located at position (u, v) in the l -layer topological layout, an edge-aware GNN can be unified as:

$$\mathbf{C}_{v,u}^l = h_l \left(\mathbf{H}_{:v}^{(l)}, \mathbf{H}_{:u}^{(l)}, \mathbf{E}_{v,u}^{(l)}, \mathbf{A} \right) \quad (4)$$

where $\mathbf{H}_{:u}^{(l)}$ and $\mathbf{H}_{:v}^{(l)}$ denotes the node embedding of node u and node v in l -th layer, and $\mathbf{E}_{v,u}^{(l)}$ represents the edge embedding of the edge connecting nodes u and v in the l -th layer. h_l is any trainable model parametrized by l .

4. Methodology

In this section, we detail the proposed method. An overview of the proposed method as well as a brief description is in Fig. 1. In general, DELs can be viewed as initial and supplementary edge features to a standard edge-aware GNN, conditioned on \mathbf{A} . In other words, DELs are *pre-calculated* only from connectivity \mathbf{A} . In Section 4.1, we introduce the way to sample a set of steady-state graph layouts following the Boltzmann distribution with local energy minima using a physics-driven graph layout algorithm. In Section 4.2, we present a simple yet effective edge embedding module to learn high-quality edge embeddings. In Section 4.3 and 4.4, we integrate these learned edge embeddings with several established GNN backbones.

4.1. Graph Layout/Configuration Sampling

A typical layout representation of \mathbf{C} is to utilize coordinates of nodes $\mathbf{P} \in \mathbb{R}^{n \times d}$ in d -dimensional space. Then there exists a mapping $\mathbf{C} = \mathbf{C}(\mathbf{P})$. Assuming that configuration \mathbf{P} conditioned on a topology/connectivity \mathbf{A} is associated with a global free energy $E(\mathbf{P}|\mathbf{A})$, we denote $E(\mathbf{P}) = E(\mathbf{P}|\mathbf{A})$ for brevity. One can sample a plausible configuration from an equipped Boltzmann distribution $\mathbb{P}(\mathbf{P}) \propto \exp(-E(\mathbf{P})/\alpha)$ using Langevin dynamics. Langevin dynamics originates from thermodynamics and has been widely used in optimization (Welling & Teh, 2011) and generative models (Song & Ermon, 2019; Shi et al., 2021). Concretely, by injecting i.i.d. Gaussian noise to the score term (Song & Ermon, 2019), the following update guarantees to sample $\mathbf{P} = \mathbf{P}_t$ from $\mathbb{P}(\mathbf{P})$ when $t \rightarrow \infty$:

$$\mathbf{P}_t = \mathbf{P}_{t-1} + \frac{\alpha}{2} \nabla_{\mathbf{P}} \log \mathbb{P}(\mathbf{P}_{t-1}) + \sqrt{\alpha} \epsilon_t, \quad \text{where } \epsilon_t \sim \mathcal{N}(0, I) \quad (5)$$

where $\alpha \rightarrow 0_+$. Note to sample from Boltzmann distribution using Langevin dynamics only requests the score term $\nabla_{\mathbf{P}} \log \mathbb{P}(\mathbf{P}_{t-1})$. Additionally, as $\nabla_{\mathbf{P}} \log \mathbb{P}(\mathbf{P}_{t-1}) = -\nabla_{\mathbf{P}} E(\mathbf{P})$ (as partition function Z does not dependent on \mathbf{P}), Eq. 5 amounts to performing gradient descent of E w.r.t. \mathbf{P} with proper additional noise. In this sense, as long as gradient term $\nabla_{\mathbf{P}} E(\mathbf{C})$ is well defined, one can readily sample \mathbf{P} from the energy surface. Specifically, when $t \rightarrow \infty$ (i.e., \mathbf{P}_t converges), $\mathbf{P} = \mathbf{P}_t$ can be viewed as a *steady-state configuration* of the free energy $E(\mathbf{P})$.

Empirically, we found that an approximation of the gradient $\nabla_{\mathbf{P}} E(\mathbf{P})$, indicating ‘‘appropriate update direction’’, is sufficient to sample satisfying \mathbf{P} for the downstream tasks in specific energy settings, while a series of energy functions are optimized alike Eq. 5. In the implementation of DEL, we employ two popularly utilized energy-based layouts in graph visualization falling into this category to sample \mathbf{P} , by further taking into account the computational overhead. We hereby introduce these algorithms. More empirical details can be found in Section 5.

Fruchterman-Reingold Layout (Fruchterman & Reingold, 1991), known as the spring-electrical model, simulates physical particle interactions involving attractive and repulsive forces. In this model, nodes are treated as charged particles, and connections as springs, with an energy function combining electrical and spring potential energy. The energy function in the spring-electrical model combines Coulomb and elastic potential energy, subjecting nodes to both attractive and repulsive forces. The negative gradient of energy

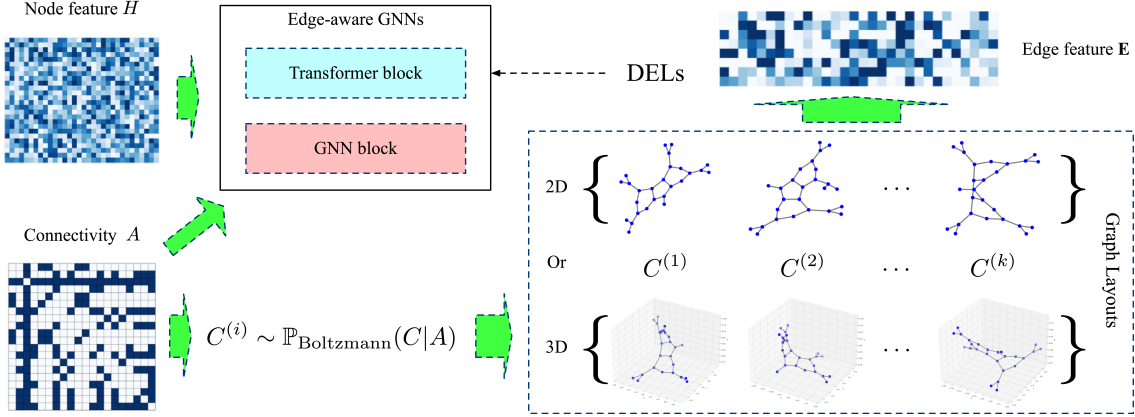


Figure 1. DEL pipeline. Our framework can be summarized into the following three steps: 1) **Sampling Layouts**: Sampling a set of layouts with local minimum energy for a given connectivity based on the Boltzmann distribution with the help of the energy-based layout algorithms. 2) **Constructing Edge Features**: Once we have a set of sampled layouts, we construct edge features based on these layouts. These edge features are designed to capture the potential energy surface of the system. Models can gain insights into the potential energy landscape and identify regions of high or low energy through the edge features. 3) **Edge-Aware GNNs**: In this final step, we combine the constructed edge features with a GNN backbone and use edge-aware GNNs to improve the performance of downstream tasks.

function can be formulated as follows:

$$-\nabla_{\mathbf{P}} E(\mathbf{P}) = k_{\text{attr}} \sum_{j \in \mathcal{N}_i} \|\mathbf{p}_i - \mathbf{p}_j\|^2 \frac{\mathbf{p}_i - \mathbf{p}_j}{\|\mathbf{p}_i - \mathbf{p}_j\|} - k_{\text{rep}} \sum_{k \neq i} \frac{\mathbf{p}_i - \mathbf{p}_k}{\|\mathbf{p}_i - \mathbf{p}_k\|^2} \quad (6)$$

Where $\mathbf{p}_i \in \mathbb{R}^d$ denotes the i -th node coordinates, k_{attr} and k_{rep} denote the attractive and repulsive force coefficients. Given that force is defined as the negative gradient of energy $-\nabla_{\mathbf{P}} E(\mathbf{P})$, force equilibria correspond to energy minima. Therefore, the spring-electrical model uses forces to iteratively move nodes until force equilibria. The iterative update process guides the layout toward lower free energy demonstrated in Fig. 3 of Appendix C.1. Algorithm 1 presents a summary of the Fruchterman-Reingold layout process. We term our method under this setting **DEL-F**.

Kamada-Kawai Layout (Kamada et al., 1989), on the other hand, only considers the spring forces on the edges. In this setting, the Kamada-Kawai Layout Algorithm connects all nodes in the graph with springs. The ideal lengths $l_{i,j}$ of these springs are determined by the shortest path distances within the original topology. Calculating the energy of the Kamada-Kawai Layout is straightforward. Given the coordinates of n particles denoted as $\mathbf{P} \in \mathbb{R}^{n \times 2}$ and the strength $k_{i,j}$ of the spring between node i and j in the 2-dimensions Euclidean plane, the position \mathbf{p}_i of i -th node represented by (x_i, y_i) , the associated energy is:

$$E = \sum_{i=1}^{n-1} \sum_{j=i+1}^n \frac{1}{2} k_{i,j} \left((x_i - x_j)^2 + (y_i - y_j)^2 + l_{i,j}^2 - 2l_{i,j} \sqrt{(x_i - x_j)^2 + (y_i - y_j)^2} \right) \quad (7)$$

The algorithm aims to minimize the energy function $E(x_1, x_2, \dots, x_n, y_1, y_2, \dots, y_n)$ through the solution of a system of $2n$ simultaneous non-linear equations (Kobourov, 2012). To find the minimum of E with respect to x_m and y_m , the Newton-Raphson method is employed. At each step, the particle \mathbf{p}_m with the largest value of Δ_m is selected, as defined below:

$$\Delta_m = \sqrt{\left(\frac{\partial E}{\partial x_m} \right)^2 + \left(\frac{\partial E}{\partial y_m} \right)^2} \quad (8)$$

For higher dimensions dim , the processing method is the same. The position of each node is fixed at each step selected by Δ_m , and the final layout algorithm produces a position matrix $\mathbf{P} \in \mathbb{R}^{n \times dim}$. More details of the layout algorithm can be found in Appendix C. Our method utilizing this layout is named as **DEL-K**.

Having sampled a set of steady-state configurations $\{\mathbf{P}^{(i)}\}_{i=1, \dots, k}$ conditioned on \mathbf{A} , our focus shifts to leveraging these steady-state configurations to boost graph representation learning. These graph configurations necessarily provide us with a global sketch of the energy surface.

Remark. Note that both the Fruchterman-Reingold layout and Kamada-Kawai layout are optimized over node coordinates/configurations \mathbf{P} , thus we need extra effort to obtain $\mathbf{C} = \mathbf{C}(\mathbf{P})$, which will be detailed in the following sections. Furthermore, there are various optional layout algorithms that can potentially be integrated with GNNs, such as spectral layout algorithms (Koren, 2003; Imre et al., 2020), hyperbolic layout algorithms (Munzner & Burchard, 1995; Munzner, 1998; Riegler et al., 2016), energy-based layout (Noack, 2009; Jacomy et al., 2014) etc., which we leave for future work.

Algorithm 1 2D Fruchterman-Reingold layout algorithm

Input: Graph $\mathcal{G} = (V, E)$ with n nodes and m edges, Iterations N , Attractive force coefficient k_{attr} , Repulsive force coefficient k_{rep} , Step size δ .

Output: Node positions matrix $\mathbf{P} \in \mathbb{R}^{n \times 2}$.

Initialize node positions matrix \mathbf{P} randomly, \mathbf{p}_i denotes the i -th node position

```

for  $i \leftarrow 1$  to  $N$  do
  foreach  $node\ v \in V$  do
    Initialize net force acting on  $v$ :  $\mathbf{F}_v \leftarrow (0, 0)$ 
    foreach  $edge\ (v, u) \in E$  do
      Calculate attractive force  $\mathbf{F}_{attr}$  between  $v$  and  $u$ :  $\mathbf{F}_{attr} \leftarrow k_{attr} \cdot \|\mathbf{p}_u - \mathbf{p}_v\|^2 \cdot \frac{\mathbf{p}_u - \mathbf{p}_v}{\|\mathbf{p}_u - \mathbf{p}_v\|}$ 
      Update  $\mathbf{F}_v$  with  $\mathbf{F}_{attr}$ 
    end
    foreach  $node\ u \in V$  do
      Calculate repulsive force  $\mathbf{F}_{rep}$  between  $v$  and  $u$  using Coulomb's law:  $\mathbf{F}_{rep} \leftarrow \frac{k_{rep}}{\|\mathbf{p}_u - \mathbf{p}_v\|} \cdot \frac{\mathbf{p}_u - \mathbf{p}_v}{\|\mathbf{p}_u - \mathbf{p}_v\|}$ 
      Update  $\mathbf{F}_v$  with  $\mathbf{F}_{rep}$ 
    end
  end
  foreach  $node\ v \in V$  do
    Update node position using net force  $\mathbf{F}_v$ :  $\mathbf{p}_v \leftarrow \mathbf{p}_v + \delta \cdot \mathbf{F}_v$ 
  end
end
    
```

4.2. Edge Features Construction via Steady-State Configurations.

As stated, directly encoding $\mathbf{P}^{(i)}$ into a graph-level feature is inappropriate, as translation and rotation do not change its inherent structure. In this section, we propose an alternative approach by transforming $\mathbf{P}^{(i)}$ into edge features based on the pairwise distance $\mathbf{D}^{(i)}$ between nodes, in accordance with the length of the springs in the graph. Specifically, the edge feature of each edge will be obtained by concatenating the length of this edge in all sampled layouts. The benefit of this edge feature is that it approximates the length distribution at which the spring reaches a steady state in all possible layouts. For the i -th layout, we can obtain an edge length matrix $\mathbf{L}^{(i)} \in \mathbb{R}^{n \times n}$ with m non-zero elements:

$$\mathbf{L}^{(i)} = \mathbf{A} \odot \mathbf{D}^{(i)}, \quad \mathbf{D}_{jk}^{(i)} = \left\| \mathbf{P}_j^{(i)} - \mathbf{P}_k^{(i)} \right\|_2 \quad (9)$$

Now we can concatenate the edge length vectors of k layouts and obtain the edge embedding $\mathbf{E} \in \mathbb{R}^{n \times n \times q}$ with q hidden dimensions through a linear layer with weight $\mathbf{W} \in \mathbb{R}^{k \times q}$ and bias $\mathbf{b} \in \mathbb{R}^q$:

$$\mathbf{E} = \mathbf{W} \cdot \left(\left[\mathbf{L}^{(1)}, \mathbf{L}^{(2)}, \dots, \mathbf{L}^{(k)} \right] \right) + \mathbf{b} \quad (10)$$

After obtaining the edge embedding \mathbf{E} , we then explore how to integrate it with the general form of GNNs.

4.3. GNNs with Edge Feature

This edge embedding \mathbf{E} derived from the steady-state layouts is an effective representation for integrating global information into the local message-passing process. We integrate the steady-state layout $\{\mathbf{C}^{(i)}\}_{i=1, \dots, k}$ into multiple existing GNN frameworks via edge features \mathbf{E} , including GAT (Veličković et al., 2018), Graph Transformer (Shi et al., 2020), and GPS (Rampášek et al., 2022). Using GAT as an example, we have employed a standard approach that concatenates node features and edge features and applied an attention mechanism to obtain node representations. We can rewrite the general form Eq. 4 of edge-aware GAT as:

$$\mathbf{C}_{v,u}^l = \frac{a_{v,u}}{\sum_{k \in \tilde{\mathcal{N}}(v)} a_{v,k}} \quad (11a)$$

$$\text{with } a_{v,u} = \exp \left(\mathbf{a}^\top \sigma \left(h_l \left[\mathbf{H}_{:v}^{(l)} \parallel \mathbf{H}_{:u}^{(l)} \parallel \mathbf{E}_{v,u}^{(l)} \right] \right) \right) \quad (11b)$$

where $\mathbf{H}_{:v}^{(l)}$ and $\mathbf{H}_{:u}^{(l)}$ represent the embeddings of nodes u and v , and $\mathbf{E}_{v,u}^{(l)} \in \mathbb{R}^d$ represents the embedding of the edge between them in l -th layer. h_l is a trainable model parametrized by l , \mathbf{a} is a parameterized weight vector, where $\alpha_{u,v}$ represents the attention score between nodes u and v , σ is a non-linear activation function. Eq. 9, 10 and 11 altogether can be viewed as an approximation of integral calculation in Eq. 2. In other words, the mapping $\mathbf{C}(\mathbf{P})$ is not explicitly calculated, the integral instead is holistically approximated. From this, we can use steady-state layout distribution to enhance GNNs. Variants of other GNN models that consider edge features can be found in Appendix E.

4.4. DEL as a Pre-processing Step

Performing sampling on each GNN layer l with Boltzmann distribution is impractical, due to not only the complexity, but also the instability and distribution shift introduced by hierarchical sampling. In our implementation, DEL is calculated only at the 0-th layer as:

$$\mathbf{H}^{(1)} = \sigma \left(\int \mathbf{C} \mathbf{H}^{(0)} \mathbf{W}^{(0)} d\mathbb{P}(\mathbf{C}) \right) \quad (12)$$

Then $\mathbf{H}^{(1)}$ is fed to the subsequent layers as a standard GNN. In this sense, DEL serves as a pre-processing step ahead of GNNs, by sampling a set of $\mathbf{P}^{(i)}$ and conducting Eq. 12 without changing any other parts.

4.5. Analysis on DEL's expressivity

We further investigate DEL's expressive power in the isomorphism test compared to variants of GNNs bounded by the 1-WL test. We have the following conclusion: The layout distribution of isomorphic graphs sampled by DEL is stable, while the layout distribution of partial non-isomorphic

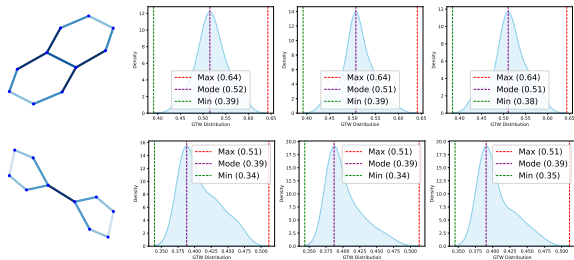


Figure 2. Comparing non-isomorphic graphs (Top: Decalin, Bottom: Bicyclopentyl) through a straightforward approach for extracting graph-level features. We sample 50 layouts to calculate graph total weights (GTW) distribution and label the minimum, maximum, and highest frequency GTWs.

graphs sampled by DEL is distinguishable. We detail our analysis in the followings.

DEL samples a set of layouts from the Boltzmann distribution with explicit energy surface. In this process, the edge length in the layout can be treated as the edge weight, producing a set of weighted graphs. To simplify our analysis, we employ the Graph Total Weight (GTW) as the representation for a layout. The GTW g_i for i -th layout is computed by summing all elements of the edge length matrix $\mathbf{L}^{(i)}$:

$$g_i = \sum_{j=1}^n \sum_{k=1}^n \mathbf{L}_{jk}^{(i)} \quad (13)$$

Then we employ Kernel Density Estimation (KDE) (Parzen, 1962) to visualize the distribution of GTW, which serves as a surrogate for the layout distribution. Our exploration centers around two non-isomorphic graphs, Decalin and Bicyclopentyl, which are indistinguishable under the 1-WL test. We run DEL multiple times and then draw KDE maps of GTW for Decalin and Bicyclopentyl. Intriguingly, as illustrated in Fig. 2, our findings reveal that the differences in layout distribution obtained from multiple runs of DEL on the isomorphic graph are negligible, which implies that DEL does not impair the expressive power of the GNNs themselves. Furthermore, we can observe that the GTW distributions of Decalin and Bicyclopentyl obtained by DEL are easily distinguishable, underscoring the effectiveness of our approach in terms of expressive power. More visualization of GTW distribution can refer to Fig. 10 in Appendix F.

5. Experiments

In this section, we extensively examine five key aspects. In Section 5.1, we present our primary results, elucidating the implementation details and performance of both our proposed method and the baseline methods. In Section 5.2, we investigate the influence of different graph layout states on the performance of DEL-F. In Section 5.3, we explore the application of DEL in high-dimensional spaces and analyze its performance in this context. In Section 5.4, we demonstrate

the impact of layout numbers on the performance of DEL. Lastly, we evaluate the computational complexity of our method and provide insights into its resource requirements for different datasets.

5.1. Main Results

Datasets. We perform experiments of graph-level tasks on widely used six datasets from TUDataset (Morris et al., 2020). Specifically, we employ two social network datasets, including IMDB-BINARY, IMDB-MULTI; and four bioinformatics datasets, including MUTAG, PROTEINS, NCI1, and D&D. In addition, we report the validation set and test set results for ogbg-molhiv dataset in the Appendix F. More details of these datasets be found in Appendix A.

Baselines. We use five graph representation learning methods as baseline models: GMT (Baek et al., 2021), SEPG (Wu et al., 2022), GIN (Xu et al., 2019b), Weisfeiler-Lehman sub-tree kernel (WL) (Shervashidze et al., 2011), GraphMAE (Hou et al., 2022). We also compare DEL with two edge feature construction methods. **Random distances** construct initial edge features with random distances and then apply our proposed edge embedding module to update the edge features. **MPNN** directly learns edge embeddings through node embeddings.

Implementation details. We applied DEL on three popular GNN backbones, including GAT (Veličković et al., 2018), Graph Transformer (Shi et al., 2020), and GPS (Rampášek et al., 2022). For GPS, we utilized the RWSE variant, which was considered to be more suitable for molecular data, while another variant, LapPE, is more suitable for images in previous work (Müller et al., 2023; Rampášek et al., 2022). Due to the presence of an MPNN mechanism in GPS, we opted not to use the corresponding MPNN variant. We developed GPS (DEL-F) and GPS (DEL-K) models that only leverage DEL for edge features. Additionally, we introduced GPS (RWSE, DEL-F) and GPS (RWSE, DEL-K) that incorporate both DEL and RWSE. To ensure a fair comparison, we followed the 10-fold cross-validation setting from previous work to obtain the model’s performance (Zhang et al., 2018; Bianchi et al., 2020; Baek et al., 2021). We then ran all methods five times with different seeds to obtain the mean and standard deviation, which are reported in Table 1. More implementation details are discussed in Appendix A.

Main Results & Analysis. In Table 1, we can find that DEL-F and DEL-K consistently improve the performance of the three GNN backbones on graph classification tasks, with DEL-F frequently achieving the best results. It’s noteworthy that previous studies (Sato et al., 2021; Wang & Zhang, 2022) have suggested that random features can sometimes improve GNN performance. To explore this, we also investigated the impact of random edge length initialization, essentially creating a random layout, within the context of DEL.

Table 1. Test performance in five graph classification datasets. Highlighted in each cell are the top **first** and **second** results. We can observe that applying DELs to three common GNN backbones leads to significant improvement, outperforming other baseline methods.

METHOD	MUTAG	NCI1	PROTEINS	D&D	IMDB-BINARY	IMDB-MULTI
WL (SHERVASHIDZE ET AL., 2011)	82.05 ± 0.36	82.19 ± 0.18	74.68 ± 0.49	79.78 ± 0.36	73.40 ± 4.63	49.33 ± 4.75
GMT (BAEK ET AL., 2021)	83.44 ± 1.33	76.35 ± 2.62	75.09 ± 0.59	78.72 ± 0.59	73.48 ± 0.76	50.66 ± 0.82
SEP-G (WU ET AL., 2022)	85.56 ± 1.09	78.35 ± 0.33	76.42 ± 0.39	77.98 ± 0.57	74.12 ± 0.56	51.53 ± 0.65
GIN (XU ET AL., 2019B)	92.31 ± 0.87	80.26 ± 0.32	75.87 ± 0.35	75.83 ± 0.65	76.41 ± 0.93	52.70 ± 0.76
GRAPHMAE (HOU ET AL., 2022)	88.19 ± 1.26	80.40 ± 0.30	75.30 ± 0.39	79.42 ± 0.42	75.52 ± 0.66	51.63 ± 0.52
GAT (VELIČKOVIĆ ET AL., 2018)	85.69 ± 1.06	77.98 ± 0.24	76.89 ± 0.37	78.12 ± 0.80	75.83 ± 0.51	52.65 ± 0.27
+RANDOM DISTANCE	79.16 ± 1.77	71.46 ± 0.76	76.41 ± 0.54	77.32 ± 0.07	76.08 ± 0.48	52.60 ± 0.58
+MPNN	84.30 ± 1.21	77.28 ± 0.27	77.18 ± 0.41	77.64 ± 0.78	75.85 ± 0.48	52.86 ± 0.29
+DEL-K	86.52 ± 0.42	77.22 ± 0.15	77.34 ± 0.35	78.78 ± 0.35	76.86 ± 0.58	52.86 ± 0.33
DEF-F	90.00 ± 0.56	78.68 ± 0.28	78.19 ± 0.58	78.89 ± 0.34	78.63 ± 0.54	53.27 ± 0.99
GRAPH TRANSFORMER (SHI ET AL., 2020)	84.02 ± 1.00	78.16 ± 0.38	77.04 ± 0.24	78.24 ± 0.46	76.43 ± 0.31	52.95 ± 0.35
+RANDOM DISTANCE	79.72 ± 0.82	69.71 ± 0.12	75.27 ± 0.13	76.97 ± 0.51	75.27 ± 0.65	52.31 ± 0.45
+MPNN	83.75 ± 1.20	78.62 ± 0.23	77.29 ± 0.68	78.26 ± 0.57	76.51 ± 0.39	52.81 ± 0.25
+DEL-K	87.77 ± 0.12	78.67 ± 0.32	78.62 ± 0.68	79.25 ± 0.11	77.65 ± 0.49	53.54 ± 0.27
DEF-F	91.52 ± 1.06	80.62 ± 0.36	78.76 ± 0.40	79.50 ± 0.15	78.28 ± 0.27	53.39 ± 0.33
GPS(RWSE) (RAMPÁŠEK ET AL., 2022)	91.94 ± 1.50	79.97 ± 0.75	74.57 ± 0.79	78.65 ± 0.52	76.45 ± 1.03	51.84 ± 0.32
GPS(LAPPE)	87.12 ± 2.37	73.88 ± 0.51	74.12 ± 1.23	77.43 ± 0.26	73.43 ± 0.56	50.31 ± 1.06
GPS(RWSE, RANDOM DISTANCE)	91.66 ± 1.74	78.98 ± 0.41	73.26 ± 0.73	77.64 ± 0.42	75.98 ± 0.67	48.28 ± 0.84
GPS(DEL-K)	91.25 ± 1.89	82.53 ± 0.41	78.42 ± 0.59	80.56 ± 0.34	77.19 ± 0.96	52.65 ± 0.27
GPS(DEL-F)	90.97 ± 0.91	82.67 ± 0.35	77.68 ± 0.99	80.38 ± 0.33	76.87 ± 1.10	52.95 ± 0.64
GPS(RWSE, DEL-K)	91.67 ± 0.88	84.22 ± 0.20	78.04 ± 0.54	81.21 ± 0.78	77.27 ± 0.93	52.90 ± 0.49
DEF-F	93.34 ± 0.68	84.36 ± 0.15	78.31 ± 0.59	81.40 ± 0.46	77.50 ± 0.65	52.86 ± 0.46

However, our experiments reveal that, within our framework, arbitrary edge layouts tend to produce a detrimental effect. Additionally, the mechanism of MPNN seems to provide limited assistance within our framework. However, since DEL relies on the topology for sampling the layout distribution, its improvements on datasets with a single consistent topology are somewhat limited, e.g., the graphs in IMDB-BINARY and IMDB-MULTI, which are ego networks with highly dense connections. Nevertheless, even within these densely connected ego networks, DEL can still identify certain distinct patterns through its layout sampling approach. For instance, in Fig. 6 of Appendix D it is observed that layout distribution tends to be more even for graphs with better symmetry and denser connections, indicating more stable topologies. Therefore, DEL still proves valuable in identifying graphs with highly similar topological structures through layout sampling.

5.2. Effect of Graph Layout Steady State on DEL Performance.

In this section, we begin by drawing average energy curves for all the graphs in the MUTAG and NCI1 datasets, considering different layout iteration steps. Next, we use performance boxplots to illustrate how GAT combined with DEL-F performs under varying iteration steps. See Fig. 8 in Appendix F, each boxplot represents results from five times runs with different random seeds. By observing the average energy curves and performance boxplots of the two datasets, we can find that both datasets optimize the energy to be lower than the random layout in a very short period (less

than five iterations) and continue to decline. As we continue to increase the steps of layout iterations, we observe a consistent trend of decreasing layout energy and improving performance.

5.3. DEL in Higher Dimensional Space

We then explore the impact of DEL in high-dimensional space. The two graph layout algorithms we employ are easily extendable to high-dimensional spaces by assigning initial random coordinates with dimensions higher than three. Here, we exemplify this extension with DEL-F. The results are presented in Table 2. Although DEL exhibited low sensitivity to changes in dimension, we noted variations in optimal dimensions across different datasets. Motivated by prior work (Noack, 2009), our investigation sought to understand how DEL’s high-dimensional aspects correlate with the optimal cluster number determined through modularity. Utilizing spectral clustering on each graph with varying cluster numbers, we relied on modularity—a widely used metric for graph clustering that assesses node tightness within clusters to evaluate clustering and identify the optimal cluster number. Our findings, presented in Table 2, suggest that, generally, higher-dimensional DEL performs better when the average number of clusters in the dataset is higher. The theoretical connection between a family of energy minimization layout algorithms in high-dimensional space and the modularity maximization problem has been extensively discussed in the literature (Noack, 2009). For more details, please refer to Appendix C.

It’s worth noting that there is no difference in the computa-

Table 2. The performance of DEL-F (GPS) with different layout dimensions. The full result can be found in Table 6.

DIMENSIONS	2	3	4	5	6	OPTIMAL CLUSTERS
MUTAG	93.34 ± 0.68	92.19 ± 1.31	92.38 ± 1.31	92.22 ± 0.87	92.36 ± 0.61	1.19
NCI1	84.25 ± 0.43	84.15 ± 0.52	83.88 ± 0.47	84.31 ± 0.40	84.10 ± 0.47	2.11
PROTEINS	77.74 ± 0.64	77.52 ± 1.10	77.88 ± 0.54	78.06 ± 0.62	77.88 ± 0.52	3.57

Table 3. Performance of DEL-F with different layout numbers.

MODEL	DATASET	LAYOUT NUMBERS				
		0	2	4	8	16
GAT	MUTAG	85.69 ± 1.06	87.91 ± 1.58	89.94 ± 1.03	89.98 ± 1.41	90.00 ± 1.18
	NCI1	77.98 ± 0.24	76.88 ± 0.51	77.49 ± 0.49	78.68 ± 0.28	78.33 ± 0.14
	PROTEINS	76.89 ± 0.37	77.56 ± 0.90	77.68 ± 0.76	77.95 ± 0.39	78.19 ± 0.58
GT	MUTAG	84.02 ± 1.00	91.25 ± 1.20	90.97 ± 0.60	91.67 ± 1.24	91.52 ± 0.16
	NCI1	78.16 ± 0.38	79.17 ± 0.39	78.46 ± 0.80	80.10 ± 0.56	80.62 ± 0.36
	PROTEIN	77.04 ± 0.24	77.47 ± 0.54	77.83 ± 0.64	78.37 ± 0.63	78.76 ± 0.40
GPS	MUTAG	91.94 ± 1.50	90.97 ± 0.82	91.25 ± 1.20	93.34 ± 0.68	90.97 ± 0.82
	NCI1	79.97 ± 0.75	83.68 ± 0.20	83.98 ± 0.54	84.31 ± 0.40	84.36 ± 0.15
	PROTEINS	74.57 ± 0.79	77.09 ± 0.77	77.38 ± 0.75	78.31 ± 0.59	77.92 ± 0.30

tional complexity of graph layout in different dimensions for the same number of iterations, and the actual time overhead is almost the same. However, higher dimensions might require more iterations to converge. Notice that another class of graph layout algorithms that easily extend to high-dimensional spaces are spectral graph layout algorithms, which we briefly discuss in Appendix C.

5.4. Effect of Different Sampling Layout Numbers on DEL Performance

In this section, we focus on the impact of the number of sampled layouts on the performance of DEL on graph classification datasets. We chose three datasets for demonstration: MUTAG, PROTEINS, and NCI1, while using DEL-F in combination with three different GNN backbones. Table 3 presents the results, showing that as the number of sampled layouts increases, there is a noticeable improvement in classification performance. This happens because DEL needs a sufficient number of sampled layouts to capture a wide range of energy distributions and better describe the inherent properties of the input topology. If we don’t sample enough layouts, DEL can’t comprehensively capture the energy surface, resulting in sub-optimal performance. But even with a small sample size, DEL still can perform better than the corresponding GNN backbone most of the time.

5.5. Computational Complexity

For the preprocessing of DEL-F, each iteration of the basic algorithm calculates attractive forces in $O(|E|)$ and repulsive forces in $O(|V|^2)$, resulting in a total computational complexity of $O(|E| + |V|^2)$. Johnson’s algo-

rithm (Johnson, 1977) is used to calculate the all-pair shortest path for DEL-K. The complexity of this calculation is $O(|V|^2 \log |V| + |V| \cdot |E|)$. We have set the maximum iteration steps to 50, following the settings of the previous work related to graph layout.

In addition to the theoretical computational complexity, we also provide the pre-processing time of DEL in practice when we sample eight layouts per graph, which can be found in Table 4. For datasets apart from D&D, we employ single-threaded processing, whereas, for D&D, we use eight parallel threads to reduce preprocessing time. It’s worth noting that higher parallelism can further save preprocessing time. Moreover, within the realm of graph layout algorithms, numerous advanced energy-based layout algorithms exist (Jacomy et al., 2014; Cheong & Si, 2020; Zhong et al., 2023), showcasing proficiency in efficiently processing large graphs. The integration of these algorithms with DEL holds the potential to significantly reduce preprocessing costs.

6. Conclusions

We propose DEL, a novel method for graph representation learning. DELs are generated by sampling topological layouts from a Boltzmann distribution on an energy surface. This approach captures a wide spectrum of global graph information and imposes additional expressivity over 1-WL-test GNNs. In the implementation, DELs serve as a pre-processing step independent of subsequent GNN architectures, making them highly flexible and applicable. By integrating DELs into several GNNs, a significant improvement over a variety of datasets can be observed, which in turn supports its potential in practice.

References

- Abboud, R., Dimitrov, R., and Ceylan, I. I. Shortest path networks for graph property prediction. In *Learning on Graphs Conference*, pp. 5–1. PMLR, 2022.
- Alon, U. and Yahav, E. On the bottleneck of graph neural networks and its practical implications. In *International Conference on Learning Representations*, 2020.
- Baek, J., Kang, M., and Hwang, S. J. Accurate learning of graph representations with graph multiset pooling. In *International Conference on Learning Representations*, 2021.
- Balcilar, M., Guillaume, R., Héroux, P., Gaüzère, B., Adam, S., and Honeine, P. Analyzing the expressive power of graph neural networks in a spectral perspective. In *Proceedings of the International Conference on Learning Representations (ICLR)*, 2021a.
- Balcilar, M., Héroux, P., Gauzere, B., Vasseur, P., Adam, S., and Honeine, P. Breaking the limits of message passing graph neural networks. In *International Conference on Machine Learning*, 2021b.
- Bianchi, F. M., Grattarola, D., and Alippi, C. Spectral clustering with graph neural networks for graph pooling. In *International conference on machine learning*, pp. 874–883. PMLR, 2020.
- Boltzmann, L. Studien über das gleichgewicht der lebenden kraft. *Wissenschaftliche Abhandlungen*, 1:49–96, 1868.
- Bouritsas, G., Frasca, F., Zafeiriou, S., and Bronstein, M. M. Improving graph neural network expressivity via subgraph isomorphism counting. *IEEE Transactions on Pattern Analysis and Machine Intelligence*, 45(1):657–668, 2022.
- Cheong, S.-H. and Si, Y.-W. Force-directed algorithms for schematic drawings and placement: A survey. *Information Visualization*, 19(1):65–91, 2020.
- Defferrard, M., Bresson, X., and Vandergheynst, P. Convolutional neural networks on graphs with fast localized spectral filtering. *Advances in neural information processing systems*, 2016.
- Dwivedi, V. P. and Bresson, X. A generalization of transformer networks to graphs. *DLG-AAAI*, 2021.
- Fruchterman, T. M. and Reingold, E. M. Graph drawing by force-directed placement. *Software: Practice and experience*, 21(11):1129–1164, 1991.
- Gansner, E. R., Koren, Y., and North, S. Graph drawing by stress majorization. In *Graph Drawing: 12th International Symposium, GD 2004, New York, NY, USA, September 29–October 2, 2004, Revised Selected Papers 12*, pp. 239–250. Springer, 2005.
- Gilmer, J., Schoenholz, S. S., Riley, P. F., Vinyals, O., and Dahl, G. E. Neural message passing for quantum chemistry. In *International conference on machine learning*, pp. 1263–1272. PMLR, 2017.
- Gong, L. and Cheng, Q. Exploiting edge features for graph neural networks. In *Proceedings of the IEEE/CVF conference on computer vision and pattern recognition*, pp. 9211–9219, 2019.
- Hamilton, W., Ying, Z., and Leskovec, J. Inductive representation learning on large graphs. 30, 2017.
- Henry, N., Fekete, J.-D., and McGuffin, M. J. Nodetrix: a hybrid visualization of social networks. *IEEE transactions on visualization and computer graphics*, 13(6):1302–1309, 2007.
- Hou, Z., Liu, X., Cen, Y., Dong, Y., Yang, H., Wang, C., and Tang, J. Graphmae: Self-supervised masked graph autoencoders. In *Proceedings of the 28th ACM SIGKDD Conference on Knowledge Discovery and Data Mining*, pp. 594–604, 2022.
- Hu, W., Fey, M., Zitnik, M., Dong, Y., Ren, H., Liu, B., Catasta, M., and Leskovec, J. Open graph benchmark: Datasets for machine learning on graphs. *Advances in neural information processing systems*, 33:22118–22133, 2020.
- Huang, N., Villar, S., Priebe, C. E., Zheng, D., Huang, C., Yang, L., and Braverman, V. From local to global: Spectral-inspired graph neural networks. *arXiv preprint arXiv:2209.12054*, 2022.
- Imre, M., Tao, J., Wang, Y., Zhao, Z., Feng, Z., and Wang, C. Spectrum-preserving sparsification for visualization of big graphs. *Computers & Graphics*, 87:89–102, 2020.
- Jacomy, M., Venturini, T., Heymann, S., and Bastian, M. Forceatlas2, a continuous graph layout algorithm for handy network visualization designed for the gephi software. *PLoS one*, 9(6):e98679, 2014.
- Jin, W., Barzilay, R., and Jaakkola, T. Junction tree variational autoencoder for molecular graph generation. In *International conference on machine learning*, pp. 2323–2332. PMLR, 2018.
- Johnson, D. B. Efficient algorithms for shortest paths in sparse networks. *Journal of the ACM (JACM)*, 24(1):1–13, 1977.

- Kamada, T., Kawai, S., et al. An algorithm for drawing general undirected graphs. *Information processing letters*, 31(1):7–15, 1989.
- Kipf, T. N. and Welling, M. Semi-supervised classification with graph convolutional networks. 2016.
- Kobourov, S. G. Spring embedders and force directed graph drawing algorithms. *arXiv preprint arXiv:1201.3011*, 2012.
- Koren, Y. On spectral graph drawing. In *International Computing and Combinatorics Conference*, pp. 496–508. Springer, 2003.
- Kreuzer, D., Beaini, D., Hamilton, W., Létourneau, V., and Tossou, P. Rethinking graph transformers with spectral attention. *Advances in Neural Information Processing Systems*, 34:21618–21629, 2021.
- Li, P., Wang, Y., Wang, H., and Leskovec, J. Distance encoding: Design provably more powerful neural networks for graph representation learning. *Advances in Neural Information Processing Systems*, 33:4465–4478, 2020.
- Liu, Q., Nickel, M., and Kiela, D. Hyperbolic graph neural networks. *Advances in neural information processing systems*, 32, 2019.
- Morris, C., Kriege, N. M., Bause, F., Kersting, K., Mutzel, P., and Neumann, M. TUDataset: A collection of benchmark datasets for learning with graphs. *arXiv preprint arXiv:2007.08663*, 2020.
- Müller, L., Galkin, M., Morris, C., and Rampásek, L. Attending to graph transformers. *arXiv preprint arXiv:2302.04181*, 2023.
- Munzner, T. Exploring large graphs in 3d hyperbolic space. *IEEE computer graphics and applications*, 18(4):18–23, 1998.
- Munzner, T. and Burchard, P. Visualizing the structure of the world wide web in 3d hyperbolic space. In *Proceedings of the first symposium on Virtual reality modeling language*, pp. 33–38, 1995.
- Noack, A. Modularity clustering is force-directed layout. *Physical review E*, 79(2):026102, 2009.
- Parzen, E. On estimation of a probability density function and mode. *The annals of mathematical statistics*, 33(3): 1065–1076, 1962.
- Rampásek, L., Galkin, M., Dwivedi, V. P., Luu, A. T., Wolf, G., and Beaini, D. Recipe for a general, powerful, scalable graph transformer. *Advances in Neural Information Processing Systems*, 35:14501–14515, 2022.
- Riegler, M., Pogorelov, K., Lux, M., Halvorsen, P., Gridwodz, C., de Lange, T., and Eskeland, S. L. Explorative hyperbolic-tree-based clustering tool for unsupervised knowledge discovery. In *2016 14th international workshop on content-based multimedia indexing (CBMI)*, pp. 1–4. IEEE, 2016.
- Rong, Y., Huang, W., Xu, T., and Huang, J. Dropedge: Towards deep graph convolutional networks on node classification. In *ICLR*, 2020.
- Sato, R., Yamada, M., and Kashima, H. Random features strengthen graph neural networks. In *Proceedings of the 2021 SIAM international conference on data mining (SDM)*, pp. 333–341. SIAM, 2021.
- Shervashidze, N., Schweitzer, P., Van Leeuwen, E. J., Mehlhorn, K., and Borgwardt, K. M. Weisfeiler-lehman graph kernels. *Journal of Machine Learning Research*, 12(9), 2011.
- Shi, C., Luo, S., Xu, M., and Tang, J. Learning gradient fields for molecular conformation generation. In *International conference on machine learning*, pp. 9558–9568. PMLR, 2021.
- Shi, W. and Rajkumar, R. Point-gnn: Graph neural network for 3d object detection in a point cloud. In *Proceedings of the IEEE/CVF conference on computer vision and pattern recognition*, pp. 1711–1719, 2020.
- Shi, Y., Huang, Z., Feng, S., Zhong, H., Wang, W., and Sun, Y. Masked label prediction: Unified message passing model for semi-supervised classification. *arXiv preprint arXiv:2009.03509*, 2020.
- Song, Y. and Ermon, S. Generative modeling by estimating gradients of the data distribution. *Advances in neural information processing systems*, 32, 2019.
- Sun, R., Dai, H., and Yu, A. W. Does gnn pretraining help molecular representation? *Advances in Neural Information Processing Systems*, 35:12096–12109, 2022.
- Sych, Y., Chernysheva, M., Sumanovski, L. T., and Helmchen, F. High-density multi-fiber photometry for studying large-scale brain circuit dynamics. *Nature methods*, 16(6):553–560, 2019.
- Topping, J., Di Giovanni, F., Chamberlain, B. P., Dong, X., and Bronstein, M. M. Understanding over-squashing and bottlenecks on graphs via curvature. In *ICLR*, 2022.
- Veličković, P., Cucurull, G., Casanova, A., Romero, A., Liò, P., and Bengio, Y. Graph attention networks. In *International Conference on Learning Representations*, 2018.

- Wang, X. and Zhang, M. How powerful are spectral graph neural networks. In *International Conference on Machine Learning*, pp. 23341–23362. PMLR, 2022.
- Wang, X., Sirianni, A. D., Tang, S., Zheng, Z., and Fu, F. Public discourse and social network echo chambers driven by socio-cognitive biases. *Physical Review X*, 10(4):041042, 2020.
- Wang, Y., Wang, Y., Sun, Y., Zhu, L., Lu, K., Fu, C.-W., Sedlmair, M., Deussen, O., and Chen, B. Revisiting stress majorization as a unified framework for interactive constrained graph visualization. *IEEE transactions on visualization and computer graphics*, 24(1):489–499, 2017.
- Welling, M. and Teh, Y. W. Bayesian learning via stochastic gradient langevin dynamics. In *Proceedings of the 28th international conference on machine learning (ICML-11)*, 2011.
- Wu, J., Chen, X., Xu, K., and Li, S. Structural entropy guided graph hierarchical pooling. In *International conference on machine learning*, pp. 24017–24030. PMLR, 2022.
- Wu, Z., Pan, S., Chen, F., Long, G., Zhang, C., and Philip, S. Y. A comprehensive survey on graph neural networks. *IEEE transactions on neural networks and learning systems*, 32(1):4–24, 2020.
- Wu, Z., Jain, P., Wright, M., Mirhoseini, A., Gonzalez, J. E., and Stoica, I. Representing long-range context for graph neural networks with global attention. *Advances in Neural Information Processing Systems*, 34, 2021.
- Xu, B., Shen, H., Cao, Q., Qiu, Y., and Cheng, X. Graph wavelet neural network. In *ICLR*, 2019a.
- Xu, K., Hu, W., Leskovec, J., and Jegelka, S. How powerful are graph neural networks? In *International Conference on Learning Representations*, 2019b.
- Xu, M., Yu, L., Song, Y., Shi, C., Ermon, S., and Tang, J. Geodiff: A geometric diffusion model for molecular conformation generation. In *ICLR*, 2021.
- Yu, T., Wang, R., Yan, J., and Li, B. Learning deep graph matching with channel-independent embedding and hungarian attention. In *International conference on learning representations*, 2019.
- Zhang, B., Luo, S., Wang, L., and He, D. Rethinking the expressive power of gnns via graph biconnectivity. In *The Eleventh International Conference on Learning Representations*, 2022.
- Zhang, G., He, H., and Katabi, D. Circuit-gnn: Graph neural networks for distributed circuit design. In *International conference on machine learning*, pp. 7364–7373. PMLR, 2019.
- Zhang, M. and Chen, Y. Link prediction based on graph neural networks. *Advances in neural information processing systems*, 31, 2018.
- Zhang, M., Cui, Z., Neumann, M., and Chen, Y. An end-to-end deep learning architecture for graph classification. In *Proceedings of the AAAI conference on artificial intelligence*, volume 32, 2018.
- Zhang, Y., Wang, X., Shi, C., Jiang, X., and Ye, Y. Hyperbolic graph attention network. *IEEE Transactions on Big Data*, 8(6):1690–1701, 2021.
- Zhong, F., Xue, M., Zhang, J., Zhang, F., Ban, R., Deussen, O., and Wang, Y. Force-directed graph layouts revisited: a new force based on the t-distribution. *IEEE Transactions on Visualization and Computer Graphics*, 2023.

Table 4. Runtime for DEL Preprocessing (seconds).

DATASET	MUTAG	NCI1	PROTEINS	DD	IMDB-BINARY	IMDB-MULTI	OGBG-MOLHIV
AVG. DEGREE	39.58	64.60	145.63	1431.31	193.06	131.87	27.5
AVG. NODES	17.9	29.8	39.1	284.3	19.8	13.0	25.5
GRAPHS	188	4,110	1,113	1,178	1,000	1,500	41,127
DEL-F	9.14	283.67	168.51	814.92	87.59	102.73	241.87
DEL-K	13.78	507.70	395.22	1944.53	154.72	124.11	394.65

A. Implementation detail

Dataset. The MUTAG dataset consists of seven kinds of graphs derived from 188 mutagenic compounds. NCI1 is a subset of balanced datasets from the National Cancer Institute, containing compounds screened for their ability to suppress human tumor cell growth. D&D contains protein structure graphs, with nodes representing amino acids and edges based on distance. PROTEINS dataset has nodes representing secondary structure elements, connected if neighboring in sequence or 3D space. IMDB-BINARY and IMDB-MULTI are movie collaboration datasets, where each graph represents actors/actresses and edges indicate their cooperation in a movie. Graphs are derived from specific movies, labeled with the movie genre. Except for the IMDB-BINARY and IMDB-MULTI datasets, other data sets have their own node features. In order to ensure a fair comparison, we use one-hot encodings of the degrees to construct the initial node features as in previous work for IMDB datasets (Baek et al., 2021; Wu et al., 2022).

Model configuration. For DEL application in three GNN backbones, we maintain the following hyperparameter settings: the learning rate is set to 5×10^{-4} , the node hidden size is set $\in \{32, 64\}$, the edge hidden size is set $\in \{16, 32, 64\}$, the batch size is set $\in \{32, 64\}$, and weight decay is set to 1×10^{-4} . We use the early stopping criterion, where we stop the training if there is no further improvement in the validation loss during 25 epochs. Furthermore, the maximum number of epochs is set to 150. In DEL, each GNN backbone is stacked with two layers and employs the Relu non-linear activation function after each layer. The corresponding original GNN, random distance variant, and MPNN variant also maintain consistent settings.

B. Discussion on graph layout algorithms and GNNs

The integration of graph layout and Graph Neural Networks (GNNs) is an area that has not been extensively explored, but there are potential connections between the two fields that can be mutually beneficial. For example, hyperbolic tree-based layout algorithms (Munzner & Burchard, 1995; Munzner, 1998; Riegler et al., 2016) aim to arrange hierarchical graphs in hyperbolic space, a concept that has also found exploration in the realm of GNNs (Liu et al., 2019; Zhang et al., 2021). Recent research in GNNs has highlighted the effectiveness of incorporating shortest path distance (SPD) to enhance the expressive power of GNNs. SP-GNN (Abboud et al., 2022), for instance, has demonstrated that GNNs using the k-SPD message passing mechanism outperform k-hop GNNs and the 1-WL test in terms of expressive power. Distance Encoding (Li et al., 2020) and SPD-WL (Zhang et al., 2022) have shown that incorporating SPD as node features can outperform the 1-WL test. Furthermore, SPD-WL has highlighted the ability to precisely identify cut edges within the graph by adding such features. Similarly, layout algorithms have recognized the importance of the shortest path distance early on. The Kamada-Kawai Layout Algorithm (Kamada et al., 1989) for example, connects all nodes in the graph with springs, and the ideal lengths $l_{i,j}$ of these springs are determined by the shortest path distances within the original topology. Another layout algorithm, the stress minimization (Gansner et al., 2005) algorithm also uses the shortest path distance as the ideal distance like the Kamada-Kawai Layout Algorithm, but it differs from the Kamada-Kawai Layout Algorithm in terms of the energy function it utilizes.

Overall, the integration of graph layout and GNNs presents a promising avenue for further exploration. The knowledge and techniques from both fields can complement each other.

C. Graph layout algorithm

In this section, we begin by providing a comprehensive overview of the Kamada-Kawai algorithm. Following that, we delve into the details of a widely employed generalized layout energy model, extensively utilized for analyzing layout effects. Lastly, we introduce the spectral layout model, showcasing its versatility and seamless extension to higher-dimensional

spaces.

The Kamada-Kawai algorithm (Kamada et al., 1989) incorporates a spring-like model into its framework, which not only applies to connected nodes but also to unconnected ones. In this algorithm, nodes are treated as if they are connected by springs, with the ideal length of these springs set to the length of the shortest path between the nodes. This approach ensures that even unconnected nodes experience a form of spring-like force, contributing to the overall layout optimization. By considering these spring forces, the algorithm iteratively adjusts the positions of all nodes to minimize the total energy, resulting in a layout that not only shortens edge lengths for connected nodes but also positions unconnected nodes in an arrangement that reflects their shortest path distances. This holistic approach enhances the overall visualization and representation of the graph’s structure. Algorithm 2 presents a summary of the Kamada-Kawai layout process.

The (a, r) -energy model for layouts. In physical systems, forces depend on the distance between interacting entities and the mass of the entities. Therefore, the essence of energy-based layout models lies in determining the relationship between forces acting on nodes and the distances between these nodes. This relationship can be linear, exponential, or logarithmic. To better comprehend and analyze energy-based layout models, Noack (2009) introduces the (a, r) -energy model. This model aims to generalize various spring-electric layout models using real numbers a and r representing attraction and repulsive forces proportional to the powers of distance d , the negative gradient of energy E of (a, r) -energy model can denote as following:

$$-\nabla_{\mathbf{P}}E(\mathbf{P}) = k_{\text{attr}} \sum_{j \in \mathcal{N}_i} \|\mathbf{p}_i - \mathbf{p}_j\|^a \frac{\mathbf{p}_i - \mathbf{p}_j}{\|\mathbf{p}_i - \mathbf{p}_j\|} - k_{\text{rep}} \sum_{k \neq i} \|\mathbf{p}_i - \mathbf{p}_k\|^r \frac{\mathbf{p}_i - \mathbf{p}_k}{\|\mathbf{p}_i - \mathbf{p}_k\|} \quad (14)$$

Where $w_{u,v}$ represents the weight of the edge $e_{u,v}$, and w_u and w_v denote the weights of nodes u and v respectively. Based on this, the Fruchterman-Rheingold layout can be described as a $(2, -1)$ -energy layout. Noack (2009) have highlighted that the value of parameter $a - r$ significantly influences the clustering density in layout design, and modularity can be seen as a special case of (a, r) -energy. Building upon this insight, several advanced layout algorithms, including LinLog $(0, -1)$ (Noack, 2009), ForceAtlas $(1, -1)$ (Jacomy et al., 2014), and others, have been introduced.

Spectral layout algorithm (Koren, 2003; Imre et al., 2020) is a graph visualization algorithm that leverages spectral theory and eigenvector decomposition. It works by constructing the Laplacian matrix from the given graph, computing its eigenvectors, and using them as coordinates to position nodes in a multi-dimensional space. The spectral layout is known for preserving the global structure and relative distances in graphs, making it valuable for visualizing large networks and finding clustering patterns in various fields such as social network analysis, bioinformatics, and recommendation systems. It can also be customized and combined with other optimization methods to refine layout results based on specific requirements.

C.1. Layout energy visualization

Since the Fruchterman-Reingold layout algorithm does not explicitly optimize the layout energy, we separately visualized the average energy of all graphs in the six data sets under different iterations of the Fruchterman-Reingold layout algorithm in Fig. 3. The average energy consists of elastic potential energy and Coulomb potential energy. We found that the trend of energy changes is consistent. Starting from the random layout iteration, the layout energy first increases and then decreases, and finally converges to the local minimum energy layout. However, we can observe that the local optimal energy of the IMDB data set is higher than the random layout. This is because the graph in the IMDB data set is a highly densely connected ego network, and there are even some fully connected graphs. These densely connected graphs tend to form layouts that cover the entire plane, resulting in stability but also high potential energy.

D. Graph layout visualization

For a given graph, we calculate multiple layouts to explore different representations. The distance between layouts generated by the same graph is measured as the average Euclidean distance of all edge lengths within each layout. This information allows us to derive a layout distance matrix, denoted as $D \in \mathbb{R}^{n \times n}$, where n is the number of layouts generated. To visualize this distance matrix, we employ a heatmap representation. To effectively compare the layout distance distributions across different graphs, we normalize the layout distances. This normalization process allows us to bring all the layout distances within a consistent range. It’s worth noting that due to normalization and the original minimum layout distance being 0 (The diagonal elements of the original distance matrix.), all elements on the heatmap that are close to 0 or close to 1 signify a highly uniform layout distribution. This implies that all layouts are either very similar or that the layout

Algorithm 2 Kamada-Kawai Algorithm

Input: Graph \mathcal{G} , Iterations N , Learning rate α

Output: Node positions for a visually pleasing layout

Initialize node positions randomly and store them in \mathbf{p} Define constants for spring force k_{attr} Set a convergence threshold (e.g., small positive value) Set a maximum number of iterations N

Calculate the shortest path distances between all pairs of nodes and store them in l_{ideal}

for $i \leftarrow 1$ **to** N **do**

foreach *node* v **do**

 Initialize net force acting on v : $\mathbf{F}_v \leftarrow (0, 0)$

foreach *edge* $e(u, v)$ **do**

 Calculate spring force \mathbf{F}_{attr} between v and u using Hooke's law: $\mathbf{F}_{attr} \leftarrow k_{attr} \cdot (||\mathbf{p}_u - \mathbf{p}_v|| - l_{ideal}[u][v]) \cdot$

$\frac{\mathbf{p}_u - \mathbf{p}_v}{||\mathbf{p}_u - \mathbf{p}_v||}$
 Update \mathbf{F}_v with \mathbf{F}_{attr}

end

end

 Calculate spring energy E_{spring} as the sum of spring forces:

$$E_{spring} = \frac{1}{2} \sum_{e(u,v) \in E} k_{attr} \cdot (||\mathbf{p}_u - \mathbf{p}_v|| - l_{ideal}[u][v])^2$$

 Calculate total energy $E = E_{spring}$

foreach *node* $v \in V$ **do**

 Compute the gradient of total energy \mathbf{E} with respect to node positions: $\nabla E_v \leftarrow \frac{\partial E}{\partial \mathbf{p}_v}$

 Update node position using gradient descent: $\mathbf{p}_v \leftarrow \mathbf{p}_v - \alpha \cdot \nabla E_v$ Or use the Newton-Raphson method to select one node at a time and solve the equation to fix its position

end

if $E < convergence_threshold$ **then**

break

end

end

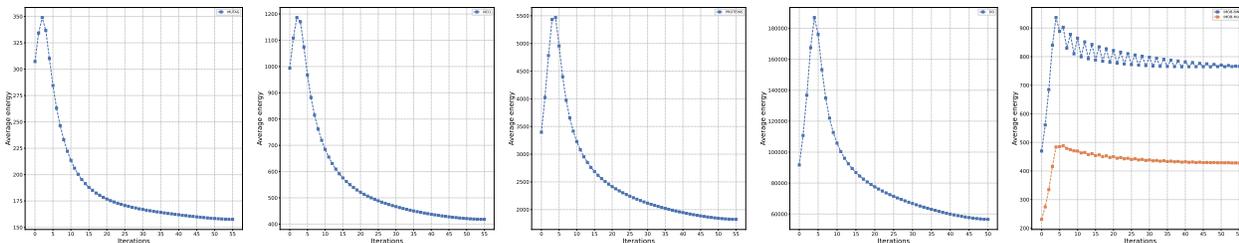


Figure 3. The layout energy change trend of the iterative process of the Fruchterman-Reingold layout algorithm for different datasets. From left to right present the average layout energy change trend of MUTAG, NCI1, PROTEINS, D&D, and IMDB datasets. In the IMDB dataset, all graphs consist of densely connected structures that tend to form layouts covering the entire plane, resulting in stability but also high potential energy.

distances are distributed evenly across the range, which is characteristic of highly concentrated or circular distributions. In order to gain a deeper insight into the layout distance distribution of a specific graph, we employ multidimensional scaling (MDS) techniques. MDS maps the layout distance matrix onto a low-dimensional space, such as a two-dimensional plane, while preserving the pairwise distances between layouts as much as possible. By visualizing the resulting MDS plot, we can observe the overall structure of the layout distance distribution, which can provide valuable insights into the characteristics of the graph. We have observed that graphs with distinct patterns often exhibit significantly different layout distance distributions. For example, in Fig. 4, our results suggest that graphs with a wider distribution of layout distances typically display folded layouts and long chains. On the other hand, graphs with a more uniform distribution of layout distances tend to feature a higher percentage of stable structures, such as rings. Similarly, in Fig. 5, we can observe that simple and stable network topologies yield uniform heatmaps and concentrated MDS clustering. These findings serve as evidence for the effectiveness of our approach in capturing and revealing patterns within molecular graphs.

It is important to note that the structure of social network graphs differs significantly from molecular graphs. Social network graphs often represent ego networks, which lack a distinct topological structure. To understand how our approach applies to these unique graph types, we have visualized the layout distance distribution of the IMDB dataset. The results, as shown in Fig. 6, clearly demonstrate that ego networks tend to exhibit highly uniform layouts due to their dense and symmetric connections. Despite the lack of a distinct structure in ego networks, we find that our topological layout algorithms can still benefit from these unique characteristics. In fact, we observe that layouts of ego networks tend to be more stable for graphs with better symmetry and denser connections, indicating more stable topologies. Furthermore, the use of MDS in two-dimensional space aids in distinguishing ego networks from other topologies and differentiating between various ego networks. These insights highlight the practical applications and advantages of our approach in different contexts.

In addition to the analysis of layout distance distributions, we also provide layout visualization examples of the six datasets we used in Fig. 7. These visualizations enable a better understanding of the unique topological structures present in different datasets. At the same time, we regularize the length of the edges in the layout and then color them. The longer the edges, the lighter the color. We can observe that the edge length is helpful in identifying those edges that connect different clusters.

E. Generic GNNs Format

Here, we provide the generic format of the graph transformer and GPS under DEL setting in Eq. 15 and Eq. 16:

$$\mathbf{C}_{v,u}^{(l)} = \text{softmax} \left(\frac{\left(\mathbf{W}_1 \mathbf{H}_{:v}^{(l)} \right)^\top \left(\mathbf{W}_2 \mathbf{H}_{:u}^{(l)} + \mathbf{W}_3 \mathbf{E}_{vu}^{(l)} \right)}{\sqrt{d}} \right) \quad (15)$$

Where \mathbf{W}_1 , \mathbf{W}_2 , and \mathbf{W}_3 are any trainable layers, d denotes the hidden dimensions of node embedding.

$$\mathbf{C}_{v,u}^{(l)} = h_l \left(\mathbf{H}_{:v}^{(l)}, \mathbf{H}_{:u}^{(l)}, \mathbf{E}_{v,u}^{(l)}, \mathbf{A} \right) + \text{GlobalAttn}^l \left(\mathbf{H}_{:v}^{(l)} \right) \quad (16)$$

Where GlobalAttn^l denotes the global attention layer in l -th layer which allows nodes to attend to all other nodes in a graph. h_l is any trainable model parametrized by l .

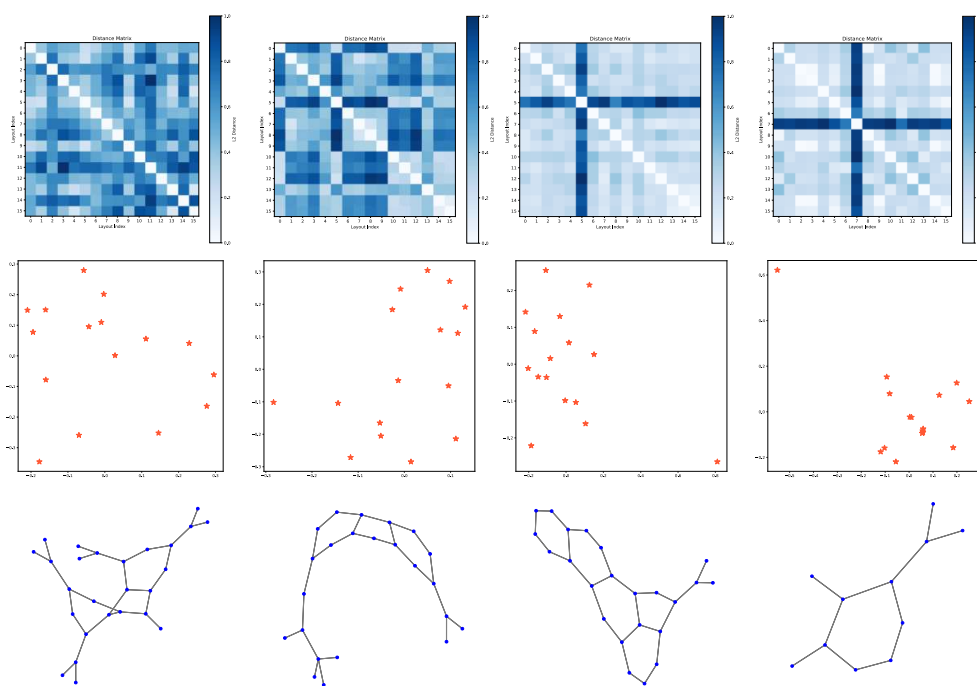


Figure 4. Heatmap, MDS layout and graph layout examples of MUTAG dataset.

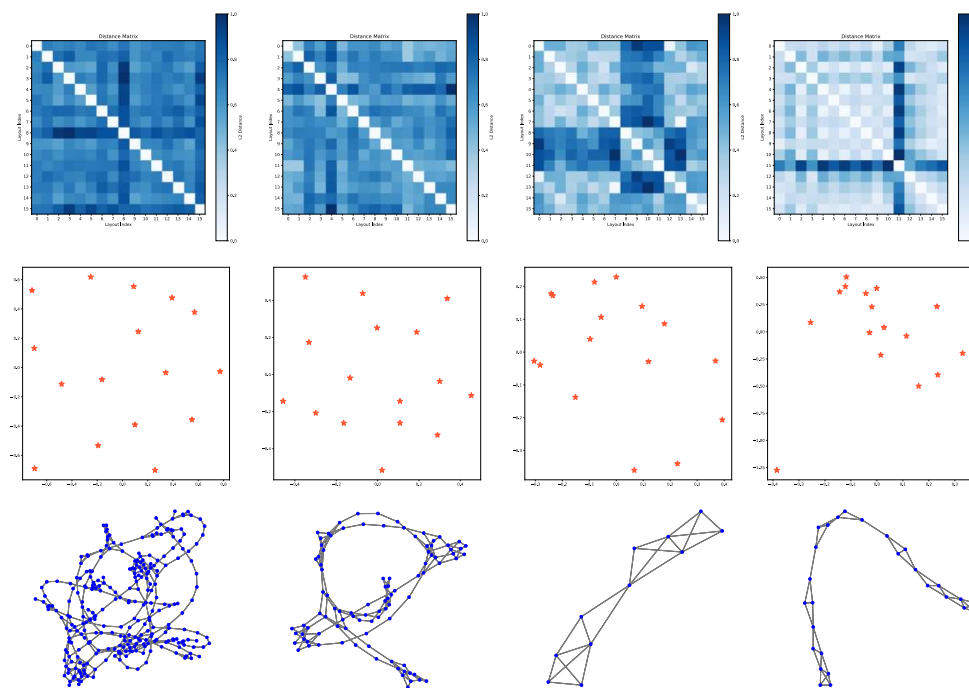


Figure 5. Heatmap, MDS layout and graph layout examples of PROTEINS dataset

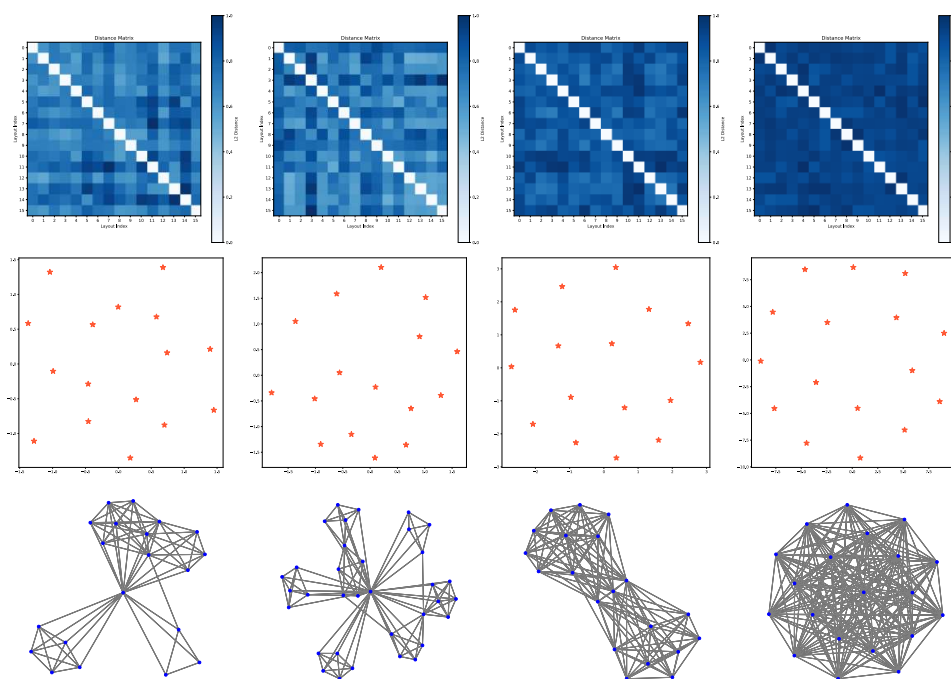


Figure 6. Heatmap, MDS layout and graph layout examples of IMDB-BINARY dataset

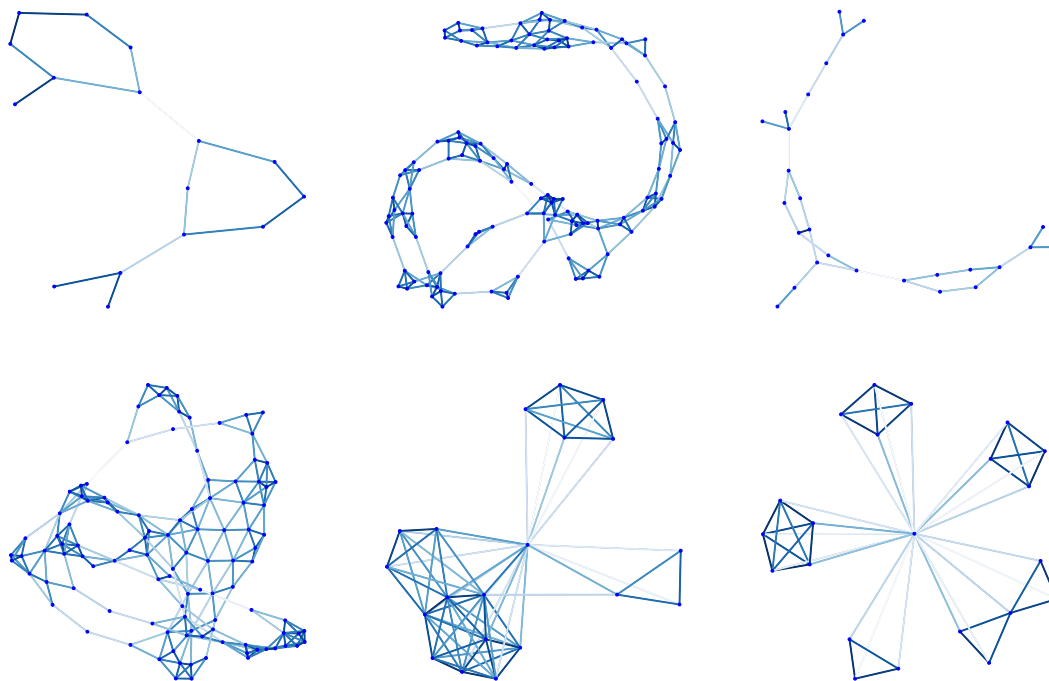


Figure 7. Graph layout examples for MUTAG, PROTEINS, NCI1, DD, IMDB-BINARY and IMDB-MULIT datasets. The longer the edges, the lighter the color. We can observe that the edge length is helpful in identifying those edges that connect different clusters.

Table 5. Valid and Test performance in ogbg-molhiv. Shown is the mean \pm std of 10 runs without any tricks. Note that ogbg-molhiv provides high-quality edge (chemical bonding) features, we simply use an MLP to fusion the edge features generated by DEL to it.

OGBG-MOLHIV	VAILD AUROC	TEST AUROC
GAT	77.67 \pm 2.78	74.45 \pm 1.53
+ DEL-K	77.42 \pm 2.15	75.24 \pm 1.24
+ DEL-F	79.34 \pm 1.36	75.47 \pm 1.05
GT	78.20 \pm 1.18	76.51 \pm 0.93
+ DEL-K	78.65 \pm 0.82	77.13 \pm 1.41
+ DEL-F	79.80 \pm 0.78	77.02 \pm 0.75
GPS	80.08 \pm 1.39	76.71 \pm 1.12
+ DEL-K	80.49 \pm 2.17	77.73 \pm 1.61
+ DEL-F	80.96 \pm 1.97	77.35 \pm 0.97

Table 6. Performance of DEL-F with different layout dimensions.

MODEL	DATASET	DIMENSIONS				
		2	3	4	5	6
GAT	MUTAG	90.00 \pm 0.56	88.61 \pm 1.59	88.33 \pm 1.11	88.61 \pm 1.49	89.98 \pm 1.41
	NCII	78.01 \pm 0.19	78.68 \pm 0.28	78.89 \pm 0.34	78.40 \pm 0.26	78.38 \pm 0.46
	PROTEINS	77.59 \pm 0.35	77.72 \pm 0.34	77.76 \pm 0.53	77.95 \pm 0.30	77.63 \pm 0.34
GT	MUTAG	90.27 \pm 1.44	91.66 \pm 1.24	90.69 \pm 0.82	90.90 \pm 1.66	91.25 \pm 1.43
	NCII	79.17 \pm 0.39	79.56 \pm 0.18	80.10 \pm 0.56	79.78 \pm 0.48	80.05 \pm 0.17
	PROTEINS(16)	78.76 \pm 0.40	78.51 \pm 0.28	78.24 \pm 0.44	77.95 \pm 0.39	78.35 \pm 0.51
GPS	MUTAG	93.34 \pm 0.68	92.19 \pm 1.31	92.38 \pm 1.31	92.22 \pm 0.87	92.36 \pm 0.61
	NCII	84.25 \pm 0.43	84.15 \pm 0.52	83.88 \pm 0.47	84.31 \pm 0.40	84.10 \pm 0.47
	PROTEINS	77.74 \pm 0.64	77.52 \pm 1.10	77.88 \pm 0.54	78.06 \pm 0.62	77.88 \pm 0.52

F. More results

In this section, we present five sets of experimental results. First, The impact of DEL on graph classification tasks when three GNNs are used as the backbones for graph layout in 2 to 6 dimensions in Table 6, We found an interesting trend that datasets with a higher optimal number of clusters(MUTAG: 1.19, NCII: 2.11, PROTEIINS: 3.57) tend to have better results when running DEL in higher dimensions. Next, we evaluated DEL’s performance on the ogbg-molhiv molecular property prediction dataset (Hu et al., 2020) (refer to Table 5), consisting of 40k graphs. Each graph represents a molecule, with nodes corresponding to atoms and edges representing chemical bonds. We observed a consistent improvement in ROC-AUC for both the validation and test sets. We employed a simple two-layer GNN architecture without special tricks, such as virtual nodes, etc., and defaulted to using Random-Walk Structural Encoding (RWSE) as a feature augmentation method. Third, we evaluated the effect of graph layout steady state on DEL-F Performance in two dataset in Fig. 8, we observe a consistent trend of decreasing layout energy and improving performance.

Beyond evaluating downstream task performance, we then delve into the expressive power of DEL. We visually examine the sampled layouts of two classical non-isomorphic maps in Fig. 9, which were previously indistinguishable by the 1-WL test but are easily discernible by DEL. This confirms that DEL’s expressive power potential surpasses that of the 1-WL test. Subsequently, we visualize seven Graph Total Weight (GTW) kernel density estimation maps for these two non-isomorphic maps in Fig. 10. Our observation reveals negligible differences in the maximum, minimum, and highest frequency GTWs within the kernel density estimation maps obtained from multiple runs of the same graph, which confirms the stability of DEL’s representation of the isomorphic graph. Distinguishing between the pair of non-isomorphic maps becomes easily achievable by scrutinizing simple statistical information in the kernel density estimation maps, such as the maximum, minimum, and highest frequency GTW.

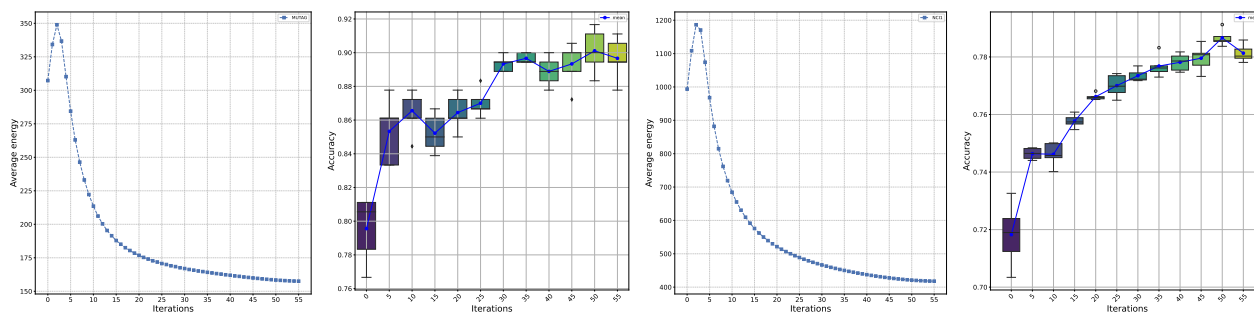


Figure 8. The average energy curve and graph classification performance of the MUTAG and NCI1 datasets under different layout iteration steps of DEL-F(GAT) are presented from left to right.

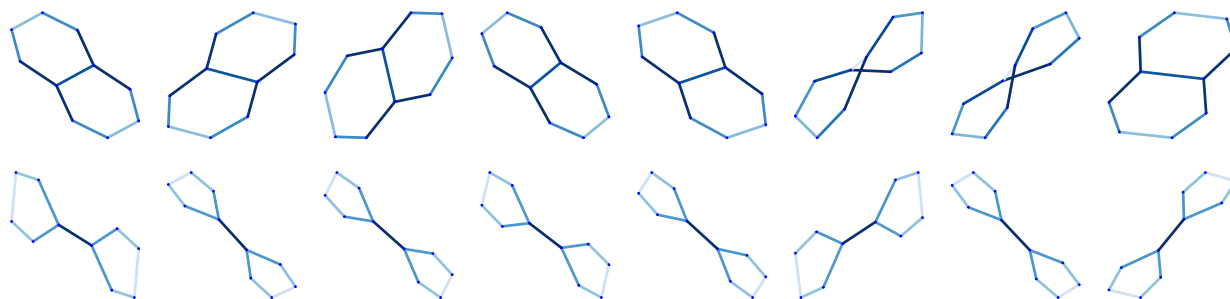


Figure 9. Layout of a pair of non-isomorphic graphs (Top: Decalin, Bottom: Bicyclopentyl). It is essential to highlight that potential layouts corresponding to a topology at a given energy are often not unique. For example, the first three layouts at the top can be considered similar and transformable through rotations, but this topology may also manifest as a folding structure, albeit with a significantly lower probability. The bottom eight layouts can be grouped into two families, with the first and sixth layouts forming one family, and the remaining layouts constituting another. Within each family, layouts can be transformed into one another through rotation or reflection. In cases of more intricate topologies, where multiple potential steady-state layouts may coexist, such scenarios become more prevalent. DEL is explicitly designed to capture a broader spectrum of global graph information, emphasizing the importance of sampling layouts from the Boltzmann distribution to avoid overlooking configurations with low probabilities that may still exist. This characteristic of DEL suggests its capability to offer a more comprehensive understanding of the graph structure.

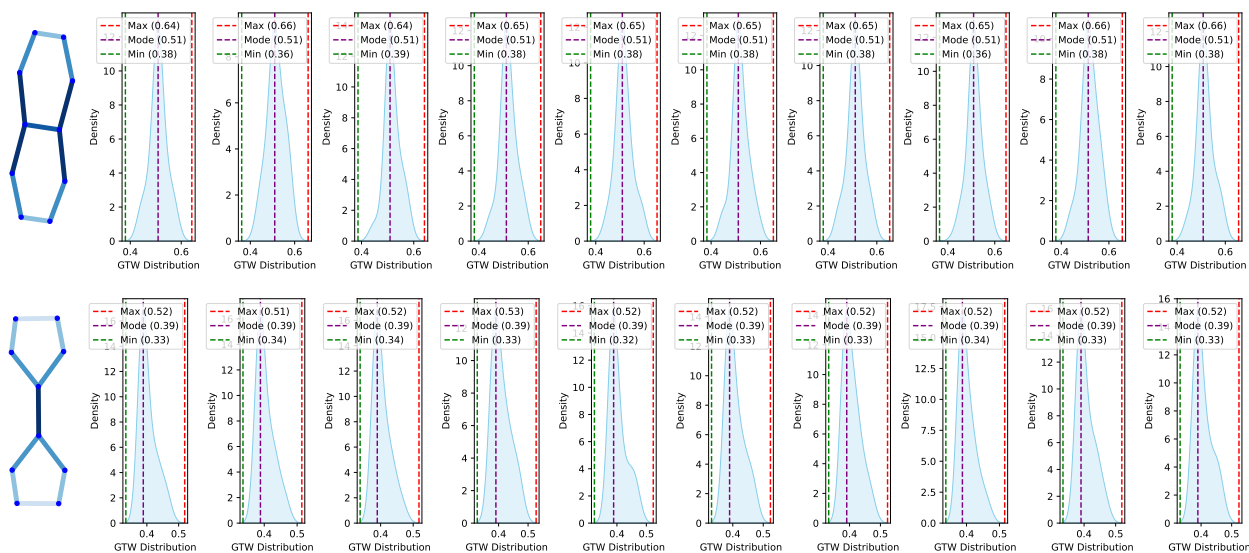


Figure 10. Comparing non-isomorphic graph (Top: Decalin, Bottom: Bicyclopentyl). We can make two key observations in this figure: 1) The graph-level features obtained from randomly computing the same topology multiple times are nearly identical. 2) Distinguishing between the Decalin and Bicyclopentyl is easily achieved using basic features such as minimum, maximum, and highest GTW.